Case Studies in Thermal Engineering 33 (2022) 101959

Contents lists available at ScienceDirect

Case Studies in Thermal Engineering

journal homepage: www.elsevier.com/locate/csite

# Transient thermal behavior in brick tunnel kiln with guide vanes: Experimental study

H.A. Refaey [a,b,*], Bandar Awadh Almohammadi [a], Ali A. Abdel-Aziz [b], H.E. Abdelrahman [b], H.A. Abd El-Ghany [c,d], Mohamed A. Karali [e], M.W. Al-Dosoky [b]

[a] Department of Mechanical Engineering, College of Engineering at Yanbu, Taibah University, Yanbu Al-Bahr, 41911, Saudi Arabia
[b] Department of Mechanical Engineering, Faculty of Engineering at Shoubra, Benha University, 11629, Cairo, Egypt
[c] Department of Engineering Mathematics and Physics, Faculty of Engineering at Shoubra, Benha University, 11629, Cairo, Egypt
[d] Department of Physics, College of Science, Taibah University, Al-Madinah Al-Munawarah, Saudi Arabia
[e] Department of Mechanical Engineering, Faculty of Engineering and Technology, Future University in Egypt, New Cairo, Egypt

ARTICLE INFO

*Keywords:*
Tunnel kiln
Bricks
Experiments
Transient
Guide vanes

ABSTRACT

Time-dependent measurements are essential to describe the temperature and heat transfer coefficient development lead to understanding the unsteady nature of tunnel kiln behavior during cooling. The present paper introduces experimental investigations in a brick tunnel kiln equipped with a U-shape guide vane to monitor its transient thermal behavior. The experimental test rig of scale 1:4 has been fabricated for this purpose. Three U-shape guide vanes have attack angles ($\theta = 120°$, 135°, and 150°) positioned in the flow direction are used to direct the flow to the confined zone among bricks columns. Two settings with a Reynolds number range from 14285 to 25480 are used. The results revealed that in absence of vanes, the average heat transfer coefficient (AHTC) has low values compared to that with vanes. The highest values of AHTC are obtained at vane angle $\theta = 135°$ , over the whole time. The Longitudinal middle bricks have the highest heat transfer coefficient for all vane angles due to high flow velocity with a good air-cooling rate. The maximum augmentation reached 48% at vane angle, $\theta = 135°$, for setting 7. The guide vanes have beneficial features when used as a turbulence generator to improve the heat transfer rate from the brick setting.

## Nomenclature

| | |
|---|---|
| a | Brick length, mm |
| $A_b$ | Brick surface area, $m^2$ |
| $A_w$ | Wet area, $m^2$ $A_w = A_{b,w} + A_{d,w}$ |
| $A_{b,w}$ | Bricks wet area, $m^2$ |
| $A_{d,w}$ | Duct wet area, $m^2$ |
| b | Brick width, mm |
| c | Brick height, mm |
| $C_p$ | Specific heat , J/kg.K |

* Corresponding author. Department of Mechanical Engineering, College of Engineering at Yanbu, Taibah University, Yanbu Al-Bahr, 41911, Saudi Arabia.
*E-mail address:* hassanein.refaey@feng.bu.edu.eg (H.A. Refaey).

https://doi.org/10.1016/j.csite.2022.101959
Received 12 January 2022; Received in revised form 14 March 2022; Accepted 19 March 2022
Available online 25 March 2022

| | |
|---|---|
| $D_h$ | Hydraulic diameter, m, $D_h = \frac{4V_f}{A_w}$ |
| f | Friction factor |
| h | Convective heat transfer coefficient $W/m^2.K$ |
| I | Electric current, Amp |
| k | Fluid thermal conductivity, W/m.K |
| L | Length of brick setting, mm |
| M | Mass flux, $kg/s.m^2$ |
| *Nu* | Nusselt number |
| P | Pressure, Pa |
| Q | Heat transfer rate, W, $Q_{input} = V_i I \cos\varnothing$ |
| $Q_{input}$ | Input heat from variac, W |
| S | Spacing between columns, m |
| u | Superficial velocity, m/s |
| U | Interstitial velocity, m/s , $U = \frac{u}{\varepsilon}$ |
| Re | Reynolds number |
| $T_{a,b}$ | Air bulk temperature, K |
| $T_{s,\,i}$ | Local brick surface temperature, K |
| $V_b$ | Bricks volume, $m^3$ |
| $V_d$ | Duct volume, $m^3$ |
| $V_f$ | Volume of flow, $m^3$, $V_f = V_d - V_b$ |
| $V_i$ | Voltage drops, Volt |

*Greek letters*

| | |
|---|---|
| θ | Attack angle |
| ε | Void fraction $\varepsilon = V_f/V_d$ |
| ρ | Density, $kg/m^3$ |
| $\rho_s$ | Setting density $= V_b/V_d$ |
| $\nu$ | Kinematic viscosity $m^2/s$ |

*Subscript*

| | |
|---|---|
| avg | average |
| i | Local value |
| mv | Middle with vanes |
| w,nv | Wall with no vanes |

*Abbreviations*

| | |
|---|---|
| AHTC | Average heat transfer coefficient |
| HTC | Heat transfer coefficient |
| LM | Longitudinal middle |
| LW | Longitudinal wall |
| TM | Transversal middle |
| TW | Transversal wall |
| $U_{vane}$ | U shape guide vanes |

## 1. Introduction

Tunnel kilns are complex structures used in ceramics and brick manufacturing. They are considered a countercurrent heat exchanger. Where the kiln car carrying bricks move in a counter direction with air or combustion gases flow. It comprises 3 zones; preheating, shooting, and the cooling zone in which the product is cooled down to near the ambient temperature [1].

Energy-saving management struggling for many researchers to study the thermal concern inside the tunnel kilns to decrease the serious energy intake. Worthy studies have been accomplished on tunnel kilns. These studies; mathematical, numerical, CFD, and experimental, included many features on the separate zones or the full kiln such as temperature profile, fuel distribution, heat transfer, and flow field.

Dugwell and Oakley [2] investigated the heat transfer progression lengthwise the kiln in which the brick column was a solid block. So, the hydrodynamic pattern was ignored nearby the bricks. Mancuhan et al. [3] presented a mathematical model to describe; gas flow, heat transfer, and water vaporization for the preheating zone. Kaya et al. [4] computed mathematically air mass flow rate and temperature profile through tunnel kiln cooling zone. The findings disclosed that the pressure drop would be minimum when the cooling zone composed two suction regions for flow and two of blowing kind.

Refaey et al. [1and5] developed mathematical models by using MATLAB for different products, bricks, and vitrified clay pipes, in tunnel kiln. The models were established to forecast temperature profiles alongside the kiln and the fuel distribution along the burning

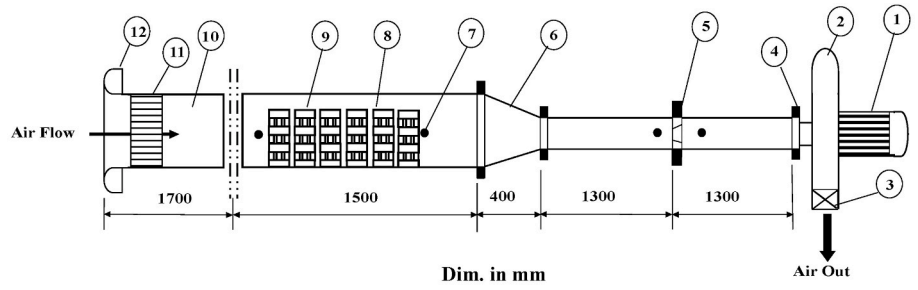


1. Electric motor
2. Air blower
3. Air gate controller
4. Flange
5. Orifice meter
6. Transition duct
7. Pressure sensors
8. Test section
9. Model arrays with guide vanes
10. Entrance duct
11. Straightener
12. Bell-mouth intake

(a)

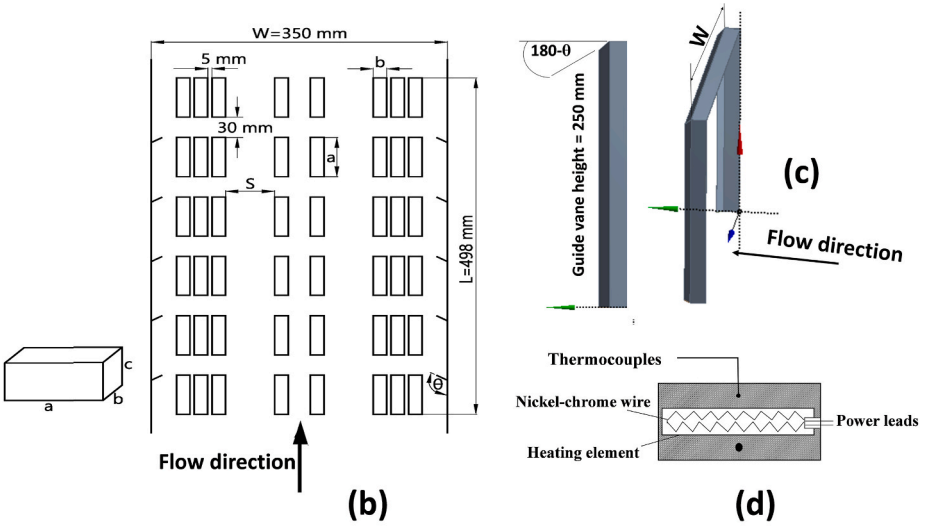


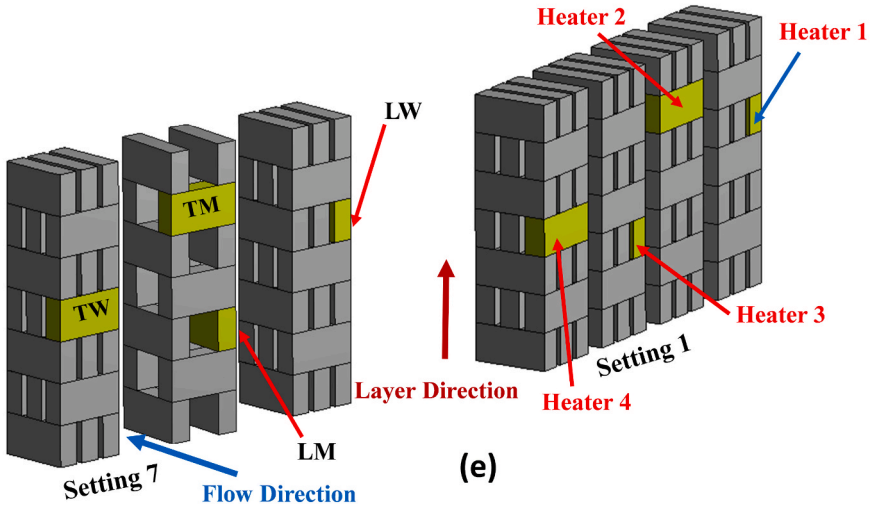


**Fig. 1.** Details of test rig represented in Ref. [16] (a) Schematic diagram (b) Setting 7 top view for the first layer (c) U shape isometric and side view (d) Heating brick model sectional view (e) Fifth row from the two settings.

zone. The model showed ordinary differential equations, ODE, to display the temperature profiles of both solids and gas. Durakovic and Delalic [6] presented a mathematical model to evaluate the stationary temperature field in both brick and kiln. Ros-Dosdá et al. [7] selected the Environmental Product Declaration (EPD) program to study the environmental life cycle valuation of diverse Porcelain stoneware tile to pinpoint the hotspots.

Nicolau et al. [8] showed 3-D numerical work and experimental thermal analysis for temperature scattering through load, gas, and walls. Naccache et al. [9] numerically examined combustion gases for both fluid flow and heat transfer inside tunnel kiln and the outcomes were compared with experimental outcomes in the literature. Santos [10] provided a numerical formulation to find tunnel kiln thermal performance with good agreement among numerical and experimental results of sawdust as a fuel. Almeida et al. [11] offered mathematical and numerical work for hollow brick drying. Refaey and Specht [12] presented three-dimensional investigations of nozzle axial velocity and arrangement to mimic the Sanitaryware products burning. The results discovered that the radial velocity formed by the burner and or nozzles was important to raise the heat transfer.

Karaush et al. [13] concluded from an experimental study that, there was an optimum spacing among the ceramic pieces and after which there was no growth in the heat absorption. Abou-Ziyan [14] established an experimental work on tunnel kiln cooling zone thermal performance. The results for the six brick settings displayed that the setting organization affects the heat transfer coefficient and pressure drop. Refaey et al. [15and16] provided new augmentation methods with two diverse guide vanes using three attack angles devoted to the kiln walls. The results were achieved for a varied range of Reynolds number and it was discovered that the convective heat transfer was powerfully dependent on the settings organization, guide vanes style, and the guide vane attack angle. Abou-Ziyan et al. [17] offered a CFD simulation around the convective heat transfer coefficients for one lattice brick setting. The results displayed that the heat transfer coefficients were enhanced by 17, 27% for the longitudinal and transverse bricks, respectively when a uniform flow is developed in the kiln.

Recently, Gomez et al. [18] quantified the transient heat transfer raised in a discontinuous ceramic kiln by a proposed methodology on a pilot-scale kiln. The results proved that using thermal insulation reduced the maximum exterior surface temperature, which dropped the thermal discomfort and work accidents during operation. Al-Hasnawi et al. [19] performed a CFD model to examine the effect of sidewall injection on gas spread in brick tunnel kilns. The space in the middle of two kiln cars was captured to simplify the study of separate gas flows, which characterized the various temperature areas for the product and the air. The results disclosed that the mixing practice was augmented by growing the vertical space among two opposing air injections. Refaey et al. [20] presented numerical investigations to mimic convective heat transfer in a brick tunnel kiln using CFD $\kappa-\omega$ BSL turbulent model. A new setting was designed and simulated. The results disclose that using CFD gives an acceptable result for new suggested settings. Ngom et al. [21] presented a numerical study using CFD for the transient cooking of clay bricks in a traditional kiln. The results verified that the supreme temperature of 900 °C was reached and the combustion process happened. Moreover, the results disclosed that the peak $O_2$ mass fraction was at the inlet and it decays regularly inside the kiln which provides evidence about combustion process spread.

From the foregoing literature, some previous studies attempt to predict the thermal behavior of a tunnel kiln in steady-state conditions. While the product load undergoes rapidly heating and cooling processes. A consequence product load inside the tunnel kiln combined with the time necessary to exchange heat with combustion gases and with air.

In the present work, a thermal analysis is provided to introduce research about a better understanding of the transient heat transfer process in the cooling zone. Guide vanes are used to decrease the thermal resistance due to the dense bricks of the products and eliminate the delays in the cooling processes. The present experimental investigation's objectives are to display the transient thermal behavior in a brick tunnel kiln. Two diverse brick settings were examined, and thermal behaviors were reported. In addition, the U shape guide vane with three various attack angles was examined. Moreover, the study intentions to offer thermal behavior data for kiln designers during their design steps for such kilns.

## 2. The experimental, test rig, procedures, and calculations

The used experimental test rig in the current work has been illustrated, designated, and presented in detail by Refaey et al. [15,16]. The representation of the test rig details is displayed in Fig. 1. The figure illustrates the current test rig used in the experimental work. One column is shown in Fig. 1a and the top view of the first layer from setting7 appears in Fig. 1b. The test section is insulated with 25 mm from glass wool to minimize the amount of heat loss through the test section. Turbulence intensity at the inlet of the tunnel must be very low as possible to study the effect of vanes correctly which improves the heat transfer process. Therefore, a bell-mouth intake, straightener, and a smooth wall are provided to remove vortex structures and eddies which reduce the turbulence intensity at the

**Table 1**
Characteristics of the present two tested settings.

| Setting | No. of Bricks | ε | $D_h$ (mm) | $A_{w,b}$ ($m^2$) | $A_{w,b}/A_{w,b1}$ (%) | $\rho_s = V_b/V_d$ | S (mm) | S/a | S/b |
|---|---|---|---|---|---|---|---|---|---|
| **1** | **504** | **0.6995** | **43.17** | **2.2936** | **100.0** | **0.3005** | **19.3** | **0.3333** | **1.2083** |
| **7** | **336** | **0.7996** | **65.77** | **1.5660** | **68.3** | **0.2004** | **58.0** | **1.0000** | **3.6250** |
| | **Reynolds number** | | | | | | | | |
| | **Re 1** | **Re 2** | | **Re 3** | **Re 4** | **Re 5** | | **Re 6** | |
| **1** | **14392** | **17164** | | **19879** | **21897** | **23345** | | **25480** | |
| **7** | **14285** | **17317** | | **19973** | **21791** | **23438** | | **25360** | |

*The brick dimensions are a = 58 mm, b = 16 mm and c = 28 mm $\rho_s$ is the setting density.

entrance to the test section. The freestream turbulence intensity was not measured and is neglected through the entrance to the test section. The top side of the test section is covered by a mild steel cover for brick replacement and guide vanes allocation, then it is closed again during executing the experiments. Four refractory bricks are used as heating in the settings. Inside each heated element, there is a 0.2 mm nickel-chrome wire wounded and cheesed in a stainless-steel probe to deliver a constant heat flux as shown in Fig. 1d. The main parameters in defining each setting could be seen in Fig. 1(b and e). The details of one row of the two settings are described in Fig. 1e. The figure displays the main limitations that identify each setting and the places of the heating elements, and the places of longitudinal and transversal plans (LW, LM, TW, and TM) used in representing the results found from the experimental work.

The U shape guide vanes are attached to the test section to direct the flow towards the enclosed zone in the rear of each row. Three attack angles for the guide vanes were used; 120°, 135°, and 150° to redirect the flow. Table 1 presents the distinguishing dimensions of the used two configurations in the present work: setting 1 and setting 7. The measurements are captured in the fifth raw [14]. Calibrated thermocouples (6 thermocouples) with accuracy ± 0.5 K (K-type) are used to measure the inlet and outlet air stream temperature (at three equally levels positioned from top to bottom). The rest thermocouples (8 thermocouples) are embedded on both sides of each heating element (1 at each surface). A data acquisition system (DAC) is used to record the instantaneous readings of the thermocouples. For pressure drop measurements, a digital differential pressure transducer (Dwyer® series WWDP, accuracy ± 2 %) is employed to measure the static pressure drop of the air among inlet and outlet through 2 mm taps located at mid-plane of the tunnel bottom surface. The investigations are studied within Reynolds number amid 14,290 and 25,480. The experimental steps are introduced for the two settings after gathering all equipment on the test rig. Furthermore, four different series of experiments are studied for each setting; one series without the guide vanes and the other three series used a U shape vane ($U_{vane}$) with three attack angles; 120°, 135°, and 150°. Then the experimental procedures are done, and readings are reported as described in Refaey et al. [16].

In the current study, 48 different experiments were performed on the two settings. The experiments were complemented under a steady-state condition when the stable fluid inlet and outlet temperatures are achieved with a determined variation of 0.5K for each thermocouple reading. The measurements of flow rate, current, voltage drop, surface temperatures of heating elements, inlet air temperature, and outlet air temperature are composed in an Excel sheet to evaluate the heat transfer and pressure drop which were calculated as represented by Refaey et al. [15and16].

The heat losses are neglected and the heat transfer rate to the flowing air is equal to the power disbursed by the heaters. The following equations represent the local and average; convective heat transfer coefficients, Reynolds number, Nusselt number, respectively as calculated by Refaey et al. [15and16]:

$$h_i = \frac{Q_{input}}{A_b\left(T_{s,i} - T_{a,\ b}\right)} \tag{1}$$

$$Re = \frac{UD_h}{\nu} \tag{2}$$

$$Nu_i = \frac{h_i D_h}{k} \tag{3}$$

Note, the index, i, refer to either longitudinal or transversal brick in the middle or nearby the wall. Additionally, the Reynolds number is established according to interstitial velocity and duct hydraulic diameter. In addition, the Darcy friction coefficient for circulated air inside the duct is calculated from the following equation.

$$f = \frac{2\Delta P D_h}{L\rho U^2} \tag{4}$$

The uncertainties were calculated rendering to the root sum square mixture of the effects of each of the single inputs as familiarized by Kline and McClintock [22]. The following equation illustrates the average uncertainty for the average Nusselt number as an example.

$$\frac{\omega_{Nu_{ave}}}{Nu_{ave}} = \pm\sqrt{\left(\frac{\omega_{h_{ave}}}{h_{ave}}\right)^2 + \left(\frac{\omega_{D_h}}{D_h}\right)^2 + \left(\frac{\omega_k}{k}\right)^2} = \pm 2.4\ \ \% \tag{5}$$

Furthermore, the bricks and duct sizes measurements were supposed to be ±0.5 mm and the uncertainty calculated to air thermal

**Table 2**
Average uncertainties in main parameters.

| Parameter | Uncertainty (ω) |
|---|---|
| u (%) | ±2.25 |
| U (%) | ±2.72 |
| Re (%) | ±3.46 |
| ΔP (%) | ±3.54 |
| f (%) | ±5.01 |
| $h_{ave}$ (%) | ±1.49 |
| $Nu_{ave}$ (%) | ±2.41 |
| Q (%) | ±2.12 |

properties is presumed to be ± 0.1%. In addition, Table 2 summarized the average uncertainties for the main parameters in the current work.

## 3. Results and discussion

Because of few studies applied for temperature development during heating and cooling processes in tunnel kiln with different brick settings. The present work is accomplished for different laying of bricks, vanes attack angles, and Reynolds number, transient conditions are considered when illustrating the temperature development and heat transfer coefficient (HTC). During the cooling progression, the solid temperature is essentially a non-steady state that always indicates the heat transfer importance from the bricks to the cooling air. Thus, the temperature time-dependent is essential when considering the cooldown of the fired bricks to their exit temperatures to avoid cracks in the products. The values of temperatures are documented through the heating and cooling processes. The confidence in the experimental setup and the measurement techniques has been presented by Refaey et al. [16].

### 3.1. Temperature profiles captured by data logger

Temperature variations of solid bricks against the time were captured by a data acquisition system, thermocouple sensors were connected to a 16-channel data acquisition system that interfaces with a computer to monitor and display the temperature readings by Pico-Log software in a datasheet or waveform chart as shown in Fig. 2. The results are presented in a normalized temperature form ($(T_{heater}-T_{air,avg})/T_{air,avg}$). For heating and cooling processes, the normalized temperatures of solid bricks are concerned of mainly

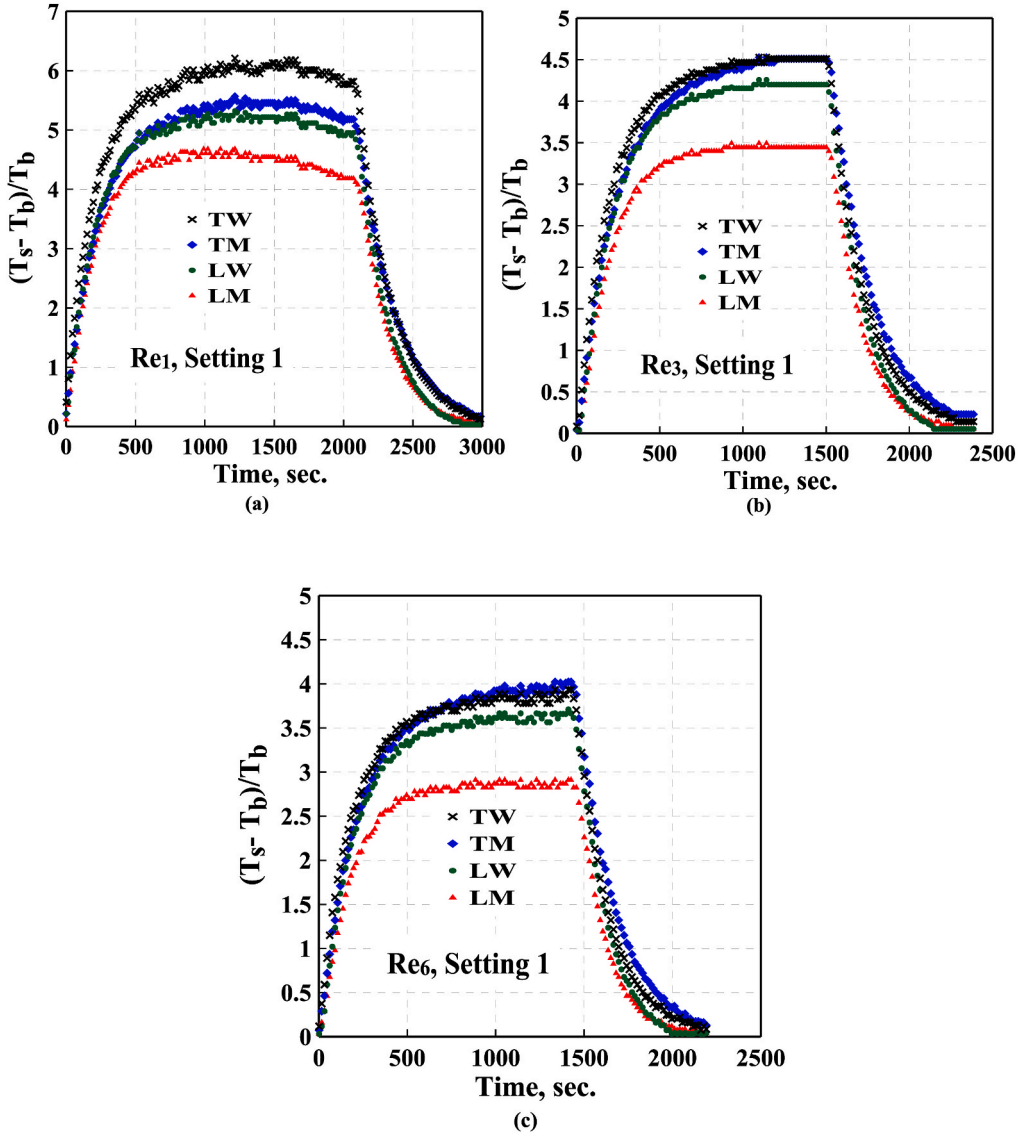


**Fig. 2.** Time variations of normalized averaged brick temperature for different brick positions and Reynolds numbers.

transverse and mid walls for setting 1 as shown in Fig. 2. It may be important to note that the solid temperatures of the bricks are affected by the position of the bricks. Time variations of the averaged brick temperatures for TW, TM, LW, and LM are compared in Fig. 2 (a, b, and c) for different Reynolds numbers, respectively.

It can be observed that, before attainment of steady-state condition, there is a significant gradient of temperature between the wall and mid bricks for transverse and longitudinal bricks in setting 1. This equilibrium has been reached for Re1 being at the heating brick process for about 1000 s, while this lasts roughly 850 s, for setting 1 being at the cooling brick process. Indeed, the temperature variation speed within the bricks is used for the heat transfer performance assessment criterion in brick settings. The effect of brick position on the normalized solid temperature is depicted in Fig. 2. The brick solid temperatures have small values for LM. Fig. 2a shows that the solid temperature is influenced by brick position during heating, which is expected to be more obvious at low values of Reynolds number. During the cooling process, Fig. 2 (a, b, and c) show that the solid brick temperatures are less sensitive to the brick positions as compared to the heating process. This can be attributed to the higher average temperature of brick grain at the startup of the cooling process and the shortened time of the cooling process in between bricks.

The transient variation of the (HTC) for different Reynolds numbers and the influence of brick position on the convective (HTC) for setting 1 is represented in Fig. 3 (a, b, and c). It can be detected that the (HTC) rapidly decreases with time and reaches steady-state condition in a shorter time for TW for higher values of Reynolds number. The main effect of guide vanes is to direct the flow towards the brick columns and subsequent influence on the boundary layer. At the beginning of cooling, the maximum heat transfer coefficient is achieved and then gradually decreased with time. The cooling rate is mainly dependent on the transient heat transfer process occurring in the thermal boundary layer and conduction in bricks. During the cooling of the bricks, the bricks are suddenly transferred

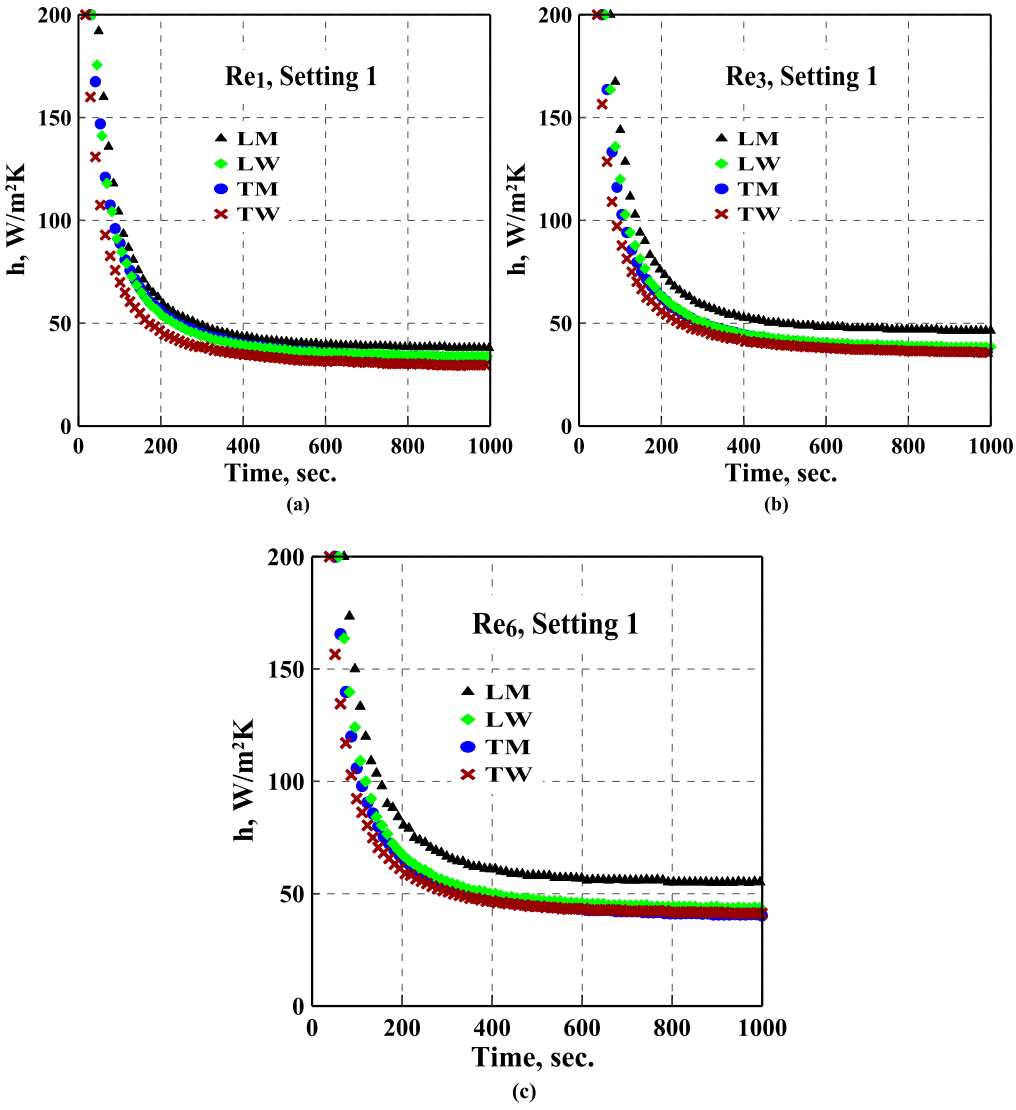


**Fig. 3.** Time variations of heat transfer coefficient for different brick positions and Reynolds numbers.

from high temperature to lower temperature. Because of the transient cooling process, at the beginning of time, the bricks will lose a great amount of heat to the cooling air, which tends to increase the air temperature at that location. However, to keep the cooling of all load bricks under uniform temperature at that location, the heat transfer coefficient improvement is required to lose the amount of heat absorbed by the load bricks.

Fig. 4 illustrates the normalized temperature variations for TW, TM, LW, and LM bricks versus the time with diverse vanes attack angles. Rows of guide vanes were devoted to the duct sidewalls to create turbulence in the airflow stream which enhances the heat transfer around bricks. The normalized brick solid temperatures will increase with time during the heating process, and no change was noticed for the normalized temperatures if the time is higher than 500 s, because the bricks reached a thermal equilibrium at steady-state conditions. The slopes of the lines prove again that the brick position has a significant effect on the brick temperatures as shown in the figure. For a given Reynolds number, the brick temperatures in presence of vanes with attack angle 135° have the lowest value compared with attack angles of 120° and 150° because of the good flow movements around bricks in the case of attack angles 120° and 135°. These results demonstrate that the vanes with 135° attack angle provide an improvement in flow distortion and blockage for different Reynolds numbers which can enhance heat transfer.

Fig. 5 shows the disparity of (HTC) versus the time for setting 1 and at Reynolds number R1. The effects of vane angles and brick location on the convective (HTC) are demonstrated in Fig. 5. The (HTC) reaches a maximum value at the beginning and steeply decreases with increasing time and approach to be nearly constant after 600 s whereas the bricks are in thermal equilibrium with surroundings. At the initial time, a very thin thermal boundary layer is generated and as a result, the heat transfer process becomes predominant by conduction. Due to the steep temperature gradient within the thermal boundary layer near the product load, the heat transfer coefficient increases greatly as the time shortens. The LM brick has the highest (HTC) for different vane angles due to high flow velocity with a good air-cooling rate in the middle. Guide vanes generate a secondary low with high turbulence of forced convection

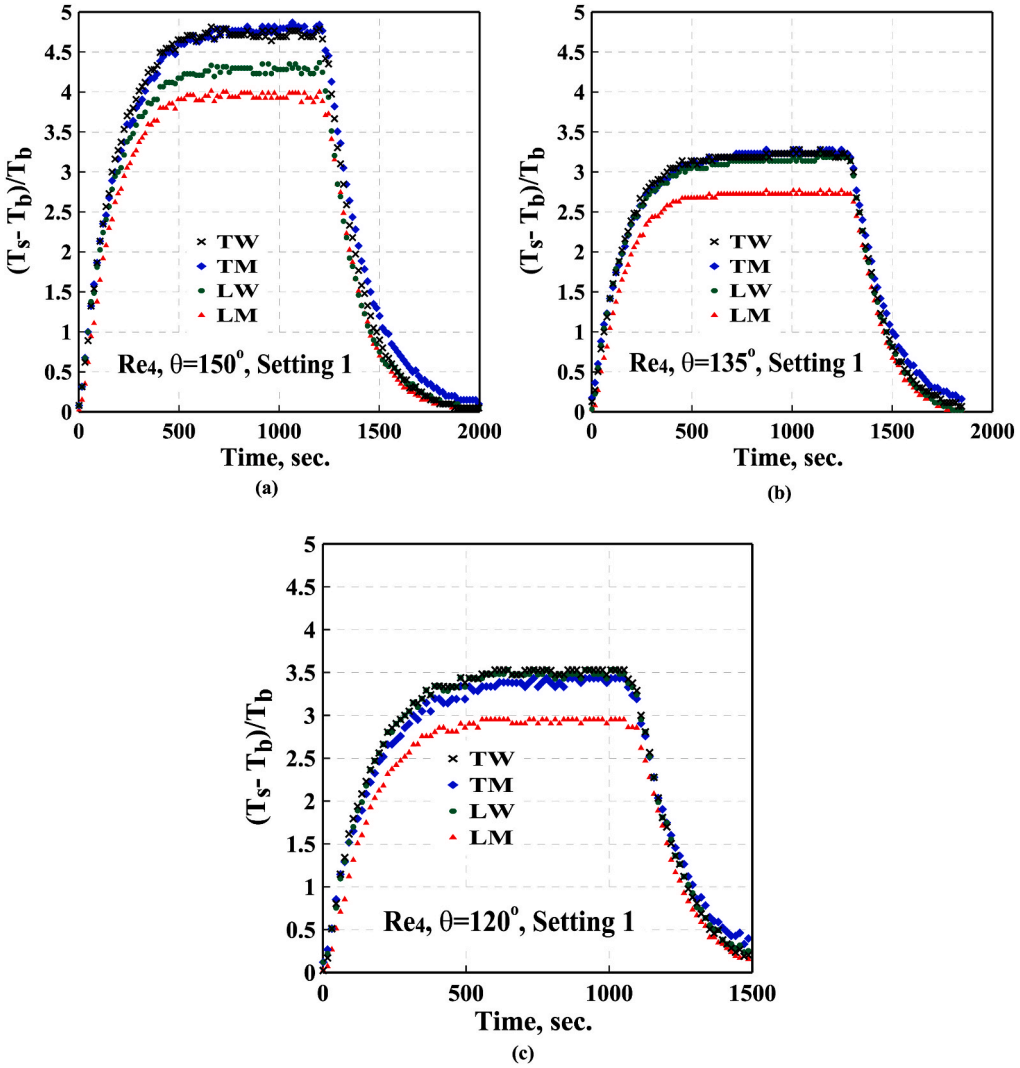


**Fig. 4.** Time variations of normalized averaged brick temperature for different vane angles during heating and cooling processes.

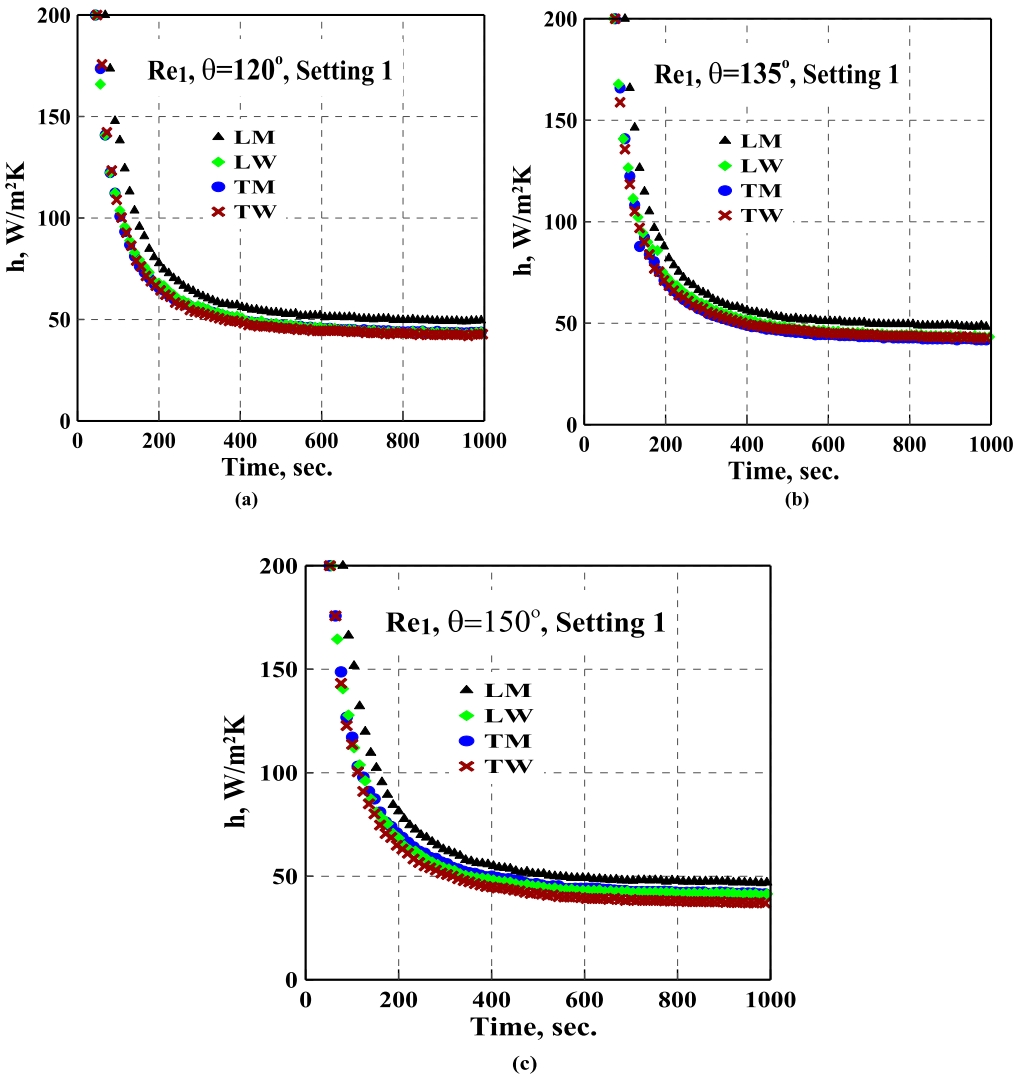


**Fig. 5.** Time variations of heat transfer coefficient for different vane angles during the heating process.

that increases the rate of heat transfer from the solid bricks.

Fig. 6 shows the time variation of the normalized temperature for different positions of bricks and different Reynolds number for setting 7. The brick solid temperatures have small values for LM. Fig. 6 demonstrates that the solid temperature is influenced by the position of the brick during heating, which is expected to be more pronounced at high values of Reynolds number. The time-dependent study is essential when considering the temperature variations of the fire bricks. This helps in the determination of the optimum position of the bricks for the constituent minerals transformation into glassy phases.

Fig. 7 presents the HTC variation against the time for setting 7 with different brick positions and Reynolds numbers. The rapid decrease in HTC with time to a steady-state condition in a shorter time is expected for higher values of Reynolds number. As expected, the (HTC) attains its maximum values at the beginning followed by a decrease approaching a nearly constant value after 500 s. The (HTC) has the highest value for LM brick for all values of Reynolds number. The LM brick position achieves nominal cooling compared with other brick positions due to the main streamwise vortices on the two sides of the brick. Also, it is observed that the brick setting 7 gives a higher heat transfer coefficient for LM at a low Reynolds number in comparison to the brick setting 1.

Fig. 8 illustrates the effect of Reynolds number on the average (HTC) for LM brick position in the two settings in absence of vane. The (HTC) decreases as the Reynolds number decreases and has the maximum values at the beginning for all values of Reynolds number in both settings. It is observed in Fig. 8a that the (HTC) has the highest values (200 $W/m^2$. K) at the beginning for all values of Reynolds number. At the initial time, the surface temperature suddenly increases and the (HTC) has the highest value because the rate of heat transfer is proportional to the temperature difference between the surfaces of brick and the air surroundings that are high at the initial time as expected. As time increases, there is a noticeable difference in heat transfer coefficient values for different values of Reynolds number. Thus, a boundary layer grows up where the temperature gradient decreases and the rate of heat transfer decreases.

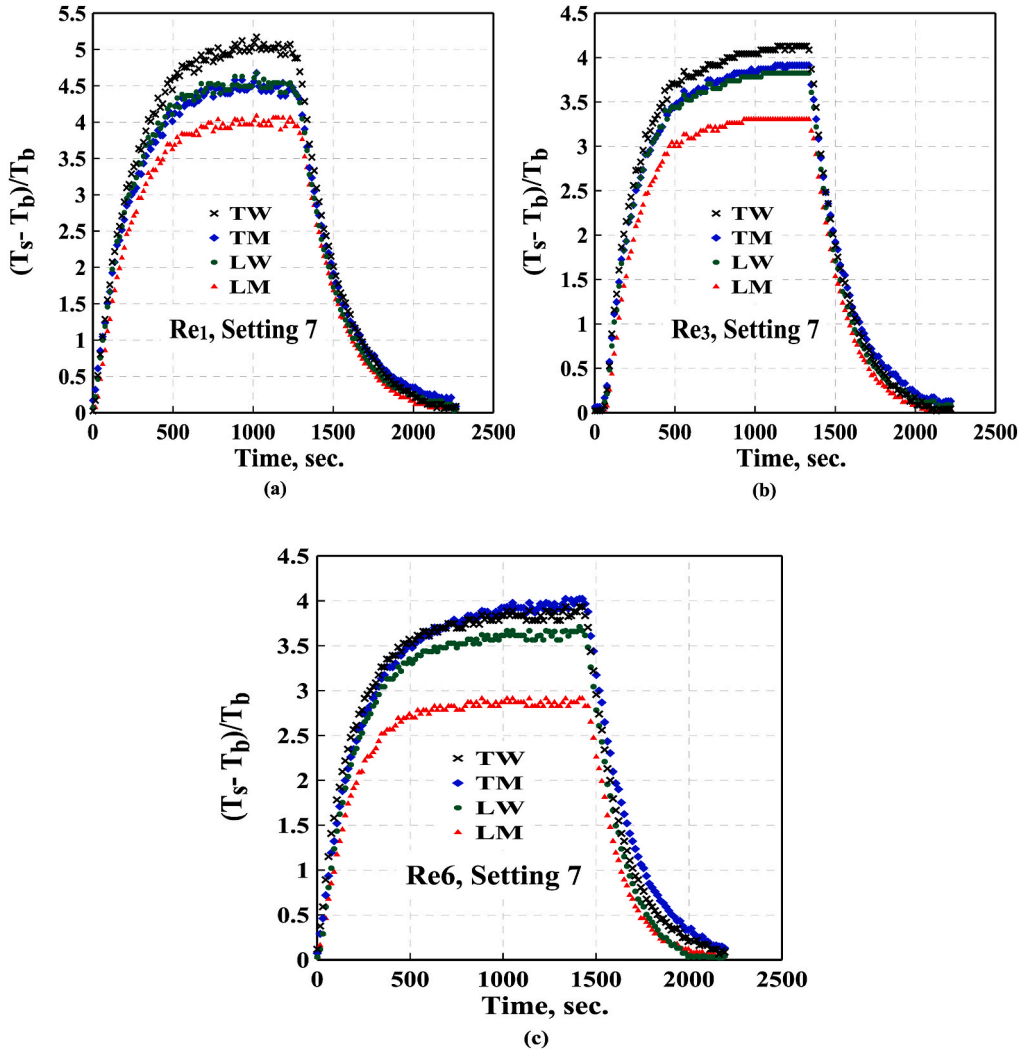


**Fig. 6.** Time variations of normalized averaged brick temperature for setting 7 with different brick positions and Reynolds numbers during heating and cooling.

Furthermore, Fig. 8b shows the time-dependent measurements for LM brick position in setting 7 in absence of vane for different values of Reynolds number. After about 400 s the curves are reversed where the heat transfer coefficients have high values at high Reynolds number, as expected. The heat transfer rate started high at the beginning and is slightly change with time after 400 s. The HTC decreases with time and reaches a steady state between 60 and 1000 min. During the first 400 s, the HTC having more vertical lines indicates a sharp decrease in its value with time. It is also observed the transformation slope for the HTC is different for different values of Reynolds number, which is crucial in studying the dynamic development of the brick walls temperatures and heat transfer coefficient.

To investigate the effects of varying vane attack angles on the average heat transfer coefficient, the duct is fitted with guide vanes on sidewalls, and results were compared in absence of vanes. Fig. 9 shows the effect of vane angles on the AHTC for the two settings. It is observed from Fig. 9a for setting 1 and Re3, that the AHTC shows great dependence upon the vane angle of attack. At the initial time, a very thin thermal boundary layer is generated and as a result, the heat transfer process becomes predominant by conduction. Due to the steep temperature gradient within the thermal boundary layer near the product load, the heat transfer coefficient increases greatly as the time shortens. It is noticed that in absence of vanes the brick setting has low values of the AHTC compared to that with vanes and the highest values at vane angle $\theta = 135^{\circ}$ over the whole time. The guide vanes have beneficial features when used as a turbulence generator to improve the heat transfer rate from the brick setting. More efficient flow blockage that produces stronger turbulence intensity is generated for the vane angle at $\theta = 135^{\circ}$ which can improve the heat transfer rate.

Fig. 9b shows the effects of vane angle on the instantaneous changes of the AHTC for different vane angles in setting 7 at the higher Reynolds number (Re6). It can be noticed a reduction in AHTC from 200 to 50 W/m$^2$.$^{o}$C. The attack angles of vanes are varied from 120° to 150°. As illustrated from the figure, using vanes with angle 135° gives the highest value (maximum enhancement 48%) of heat transfer coefficient which is more than that of the 120° and 150°. Therefore, the investigated vane angle is effective for improving the

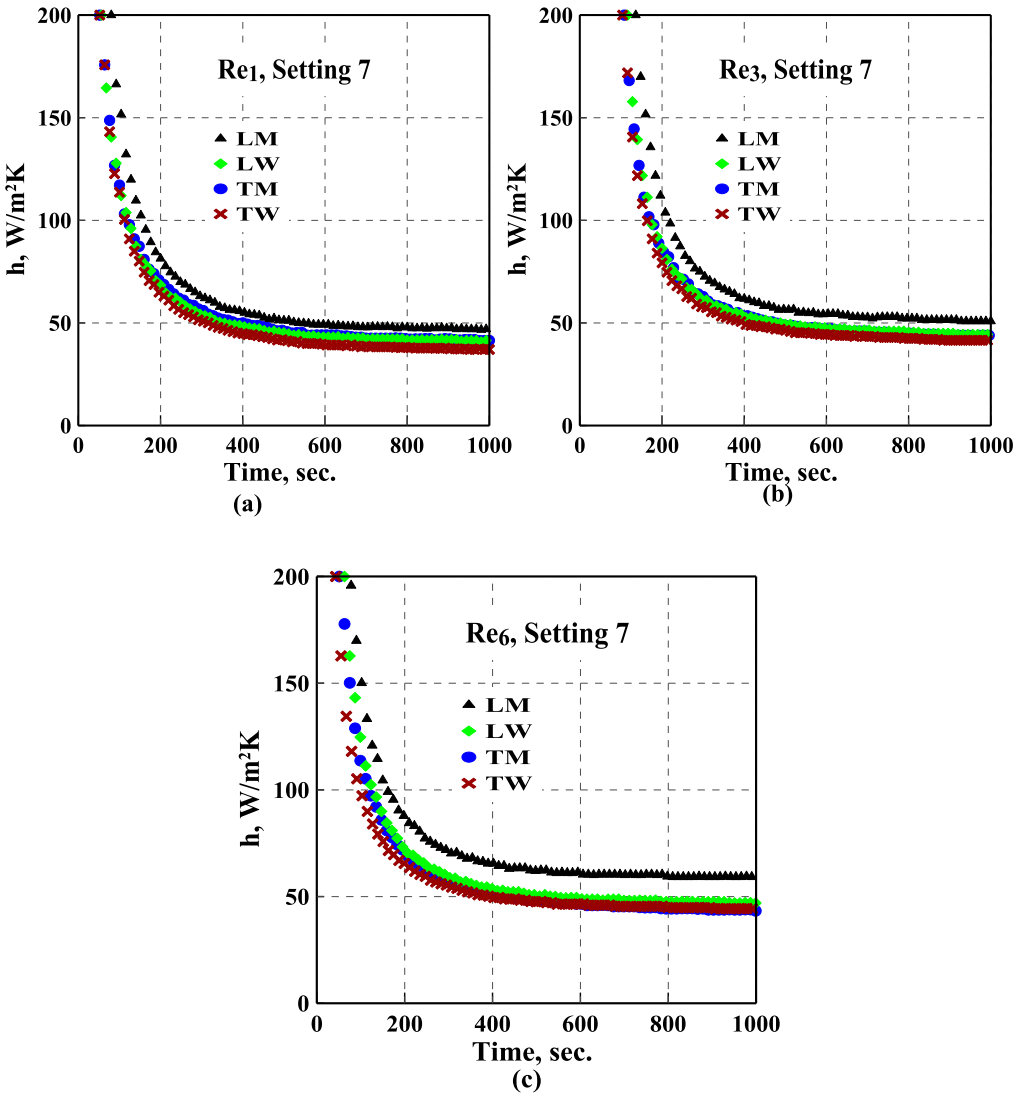


**Fig. 7.** Time variations of heat transfer coefficient for setting 7 with different brick positions and Reynolds numbers during the heating process.

AHTC. In addition, for vane angle 150°, the AHTC is almost the same as that obtained in absence of vanes. Therefore, no need to use the vanes with angle 150°, especially due to the pressure drop associated with it.

Fig. 10 shows the instantaneous variation of heat transfer coefficient for setting 7 with different vane angles for both heating and cooling processes. The cooling process was much faster requiring about 300 s to reach a steady state while the heating process needs about 800 s to reach a steady state. The bricks with high temperatures release heat fast to the cooling air. Also, the thermal mass of bricks has some influences on the instantaneous change of heat transfer coefficient which refers to the ability of a material to absorb, store and release heat drop associated with it. For different vane angles and during the cooling process, the conduction in bricks tends to be stable when time increases. The amount of heat convective to the coolant decreases gradually and tends to be stable while the cooling air temperature also increases gradually and tends to be stable until asymptotic time. Because a much energy is wasted in cooling zones that undergo a positive pressure. Therefore, heat transfer enhancement is required in the cooling zones to save energy.

## 4. Conclusions

The transient monitoring of the convective heat transfer during heating and cooling of the brick tunnel kiln is simulated experimentally in the current work. Guide vanes with different attack angles are equipped to the kiln, providing an enhancement in convective heat transfer coefficient. That indicates a short time for cooling airflow and provides a high measure of energy saving. The thermal performance of the heating and cooling is experimentally investigated for two different brick settings (1 &7). Furthermore, an augmentation method using U shape guide vanes ($U_{vane}$) with different attack angles 120°, 135°, and 150° are offered.

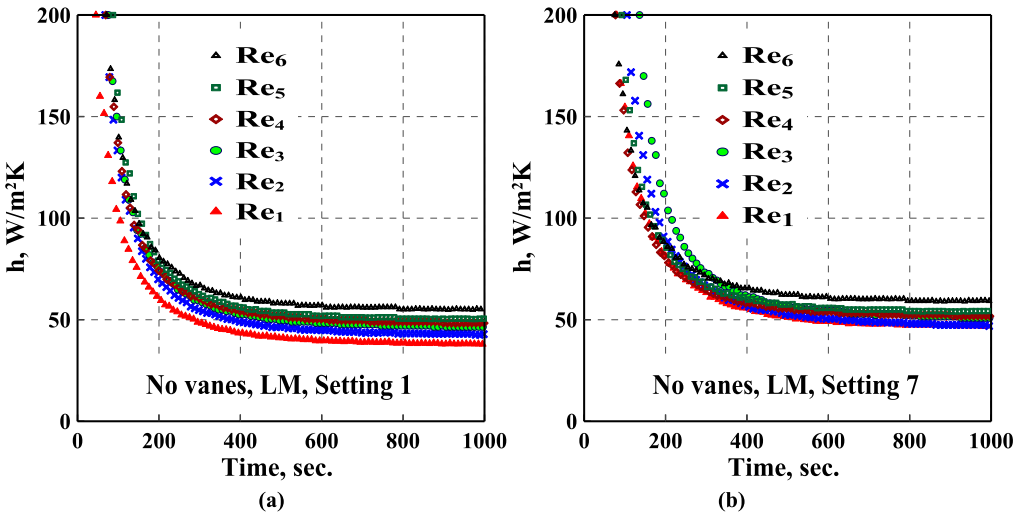


**Fig. 8.** Time variations of heat transfer coefficient for different Reynolds numbers for no vanes (a) Setting 1 (b) Setting 7.

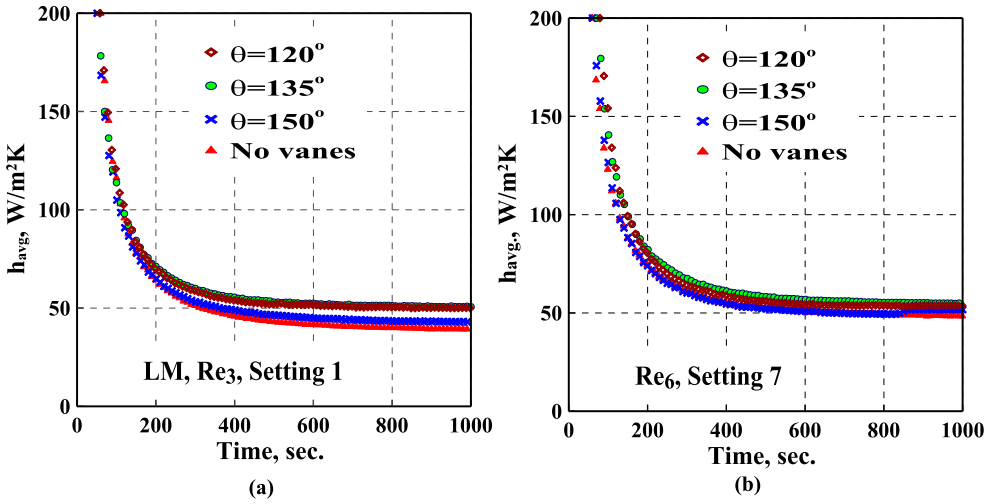


**Fig. 9.** Time variations of heat transfer coefficient for different vanes angles (a) Setting 1 (b) Setting 7.

The following arguments could be drawn from the experimental results:

- For the two bricks settings, the attack angle vanes ($U_{vane}$) have an excessive impact on the average heat transfer coefficient.
- It is noticed that at the beginning, in absence of vanes the brick setting has low values of the AHTC compared to that with vanes, and the highest values at vane angle $\theta = 135^{\circ}$ over the whole time.
- The guide vane improves the flow characteristics around a longitudinal middle brick and thus the heat transfer rate increases in comparison to the bricks in the wall column.
- The (HTC) reaches a supreme value at the beginning and steeply decreases with increasing time and approach to be nearly constant after 600 s whereas the bricks are in thermal equilibrium with surroundings.
- The LM brick has the highest (HTC) for different vane angles due to high flow velocity with a good air-cooling rate in the middle.
- Guide vanes generate a secondary low with high turbulence of forced convection that increases the rate of heat transfer from the solid bricks.
- The maximum improvement in heat transfer rate touched 48% for setting 7 compared with that in absence of guide vanes for $\theta = 135^{\circ}$ compared to setting 1.
- As the vane attack angle diminutions, the average heat transfer rate grows.
- The present research offers some solutions for the thermal engineering design of tunnel kilns without increasing the dimensions of the tunnel. In the cooling zone, a transformation of the quartz phase occurs at a critical temperature through the product material, it is important to prevent product collapses by controlling the cooling velocity. To increase the cooling rate and production, an air

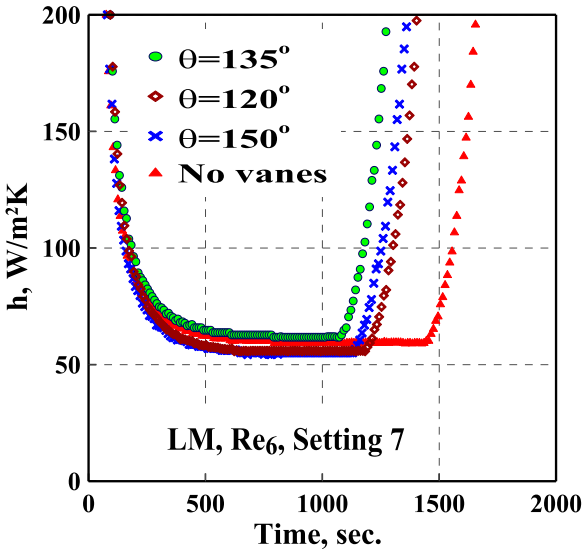


**Fig. 10.** Instantaneous change of heat transfer coefficient during heating and cooling processes for different vane angles (θ) in setting 7.

injection onto the product is required to attain a sudden reduction in the temperature in the cooling zone which requires more energy consumption. Therefore, transient thermal analysis is performed for the product in which varying the guide vane attack angles promotes a more uniform cooling process with less energy consumption.

## CRediT authorship contribution statement

**H.A. Refaey:** Management and coordination responsibility for the research activity planning and execution, Conceptualization, Experimental work execution and analysis, Data collection, Writing – original draft, Manuscript preparation, Formal analysis. **Bandar Awadh Almohammadi:** Conceptualization, Literature survey, Writing and manuscript editing. **Ali A. Abdel-Aziz:** Management and coordination responsibility for the research activity planning and execution, Formal analysis, and discussion, Manuscript Writing and data, Formal analysis. **H.E. Abdelrahman:** Management and coordination responsibility for the research activity planning and execution, Conceptualization, Experimental work execution, Manuscript preparation, Formal analysis. **H.A. Abd El-Ghany:** Conceptualization, Writing and manuscript editing. **Mohamed A. Karali:** Conceptualization, Literature survey, Writing and manuscript editing. **M.W. Al-Dosoky:** Conceptualization, Experimental work execution, Formal analysis, Data collection, Writing – original draft, Manuscript preparation, Formal analysis.

## Declaration of competing interest

The authors declare that they have no known competing financial interests or personal relationships that could have appeared to influence the work reported in this paper.

## References

[1] H.A. Refaey, Mathematical Model to Analyze the Heat Transfer in Tunnel Kilns for Burning of Ceramics, Otto- von Guericke University, Magdeburg, Germany, 2013. Ph.D. dissertation.
[2] D.R. Dugwell, D.E. Oakley, A model of heat transfer in tunnel kilns used for firing refractories, Int. J. Heat Mass Tran. 31 (11) (1988) 2381–2390.
[3] E. Mancuhan, K. Kucukada, E. Alpman, Mathematical modeling and simulation of the preheating zone of a tunnel kiln, J. Therm. Sci. Technol. 31 (2) (2011) 79–86.
[4] S. Kaya, K. Kucukada, E. Mancuhan, Model-based optimization of heat recovery in the cooling zone of a tunnel kiln, Appl. Therm. Eng. 28 (2008) 633–641.
[5] H.A. Refaey, Mohamed A. Karali, Adnan G. Al-Hasnawi, Eckehard Specht, in: Mathematical Model to Simulate the Heat Transfer in Vitrified Clay Pipes Kiln, Conference Paper: International Conference on Applied Mechanics and Mechanical Engineering, AMME-18, Military Technical College, Cairo, Egypt, 2018, 03 - 05 April.
[6] J. Durakovic, S. Delalic, Temperature field analysis of tunnel kiln for brick production, Mater. Geoenviron 53 (3) (2006) 403–408.
[7] T. Ros-Dosdá, I. Celades, E. Monfort, Environmental profile of Spanish porcelain stoneware tiles, Int. J. Life Cycle Assess. (2017).
[8] V. de Paulo Nicolau, A.P. Dadam, Numerical and experimental thermal analysis of a Tunnel Kiln used in ceramic production, J. Braz. Soc. Mech. Sci. Eng. 31 (4) (2009) 297–304.
[9] M.F. Naccache, M.S.P. Gomes, A.O. Nieckele, Numerical Simulation of Flow and Heat Transfer through a Tunnel Kiln, 18th International Congress of Mechanical Engineering November 6-11, Ouro Preto, MG, 2005.
[10] G.M. Santos, Study of Thermal Behavior of a Tunnel Kiln Used in Red Ceramic Industry (in portuguese), Federal University of Santa Catarina, Santa Catarina, Brazil, 2001. M.Sc. dissertation.
[11] G.S. Almeida, J.B. Silva, C.J. Silva, R. Swarnakar, G.A. Neves, A.G. Lima, Heat and mass transport in an industrial tunnel dryer: modeling and simulation applied to hollow bricks, Appl. Therm. Eng. 55 (2013) 78–86.
[12] H.A. Refaey, E. Specht, Flow field visualization to simulate the burning of sanitaryware in tunnel Kilns, in: Proceedings of ICFD11: Eleventh International Conference of Fluid Dynamics December, 19–21, 2013 (Alexandria, Egypt).

[13] S.A. Karaush, Y.I. Chizhik, E.G. Bober, Optimization of ceramic setting as a function of their heat absorption from the radiating walls of the furnace, Glass Ceram. 54 (5) (1997) 190–192.
[14] H.Z. Abou-Ziyan, Convective heat transfer from different brick arrangements in tunnel Kilns, Appl. Therm. Eng. 24 (2004) 171–191.
[15] H.A. Refaey, Ali A. Abdel-Aziz, R.K. Ali, H.E. Abdelrahman, M.R. Salem, Augmentation of convective heat transfer in the cooling zone of brick tunnel kiln using guide vanes: an experimental study, Int. J. Therm. Sci. 122 (2017) 172–185.
[16] H.A. Refaey, Ali A. Abdel-Aziz, M.R. Salem, H.E. Abdelrahman, M.W. Al-Dosoky, Thermal performance augmentation in the cooling zone of brick tunnel kiln with two types of guide vanes, Int. J. Therm. Sci. 130 (2018) 264–277.
[17] Hosny Z. Abou-Ziyan, Issa F. Almesri, Mosab A. Alrahmani, Jaber H. Almutairi, Convective heat transfer coefficients of multifaceted longitudinal and transversal bricks of lattice setting in tunnel kilns, J. Therm. Sci. Eng. Appl. 10 (2018) 1–13, 51014.
[18] Ricardo S. Gomez, Túlio R.N. Porto, Hortência L.F. Magalhães, Gicelia Moreira, M. Anastácia, M.C.N. André, Ruth B.F. Melo, Antonio G.B. Lima, Natural gas Intermittent Kiln for the ceramic Industry: a transient thermal analysis, Energies 12 (2019) 15681–156829.
[19] A.G.T. Al-Hasnawi, H.A. Refaey, T. Redemann, T. Attala, E. Specht, Computational fluid dynamics simulation of flow mixing in tunnel Kilns by air side injection, J. Therm. Sci. Eng. Appl. 10 (3) (2018) 31007, https://doi.org/10.1115/1.4038840. June.
[20] H.A. Refaey, Mathkar A. Alharthi, M.R. Salem, Ali A. Abdel-Aziz, H.E. Abdelrahman, M.A. Karali, Numerical investigations of convective heat transfer for lattice settings in brick Tunnel Kiln: CFD simulation with experimental validation, Therm. Sci. Eng. Prog. 24 (2021).
[21] M. Ngom, A. Thiam, A. Balhamri, V. Sambou, T. Raffak, H.A. Refaey, Transient study during clay bricks cooking in the traditional kiln; CFD numerical study, Case Stud. Therm. Eng. 28 (2021).
[22] S.J. Kline, F.A. McClintock, Describing uncertainties in single-sample experiments, Mech. Eng. 75 (1) (1953) 3–8.